PCCP

Physical Chemistry Chemical Physics

rsc.li/pccp

25 YEARS ANNIVERSARY

ROYAL SOCIETY
OF CHEMISTRY
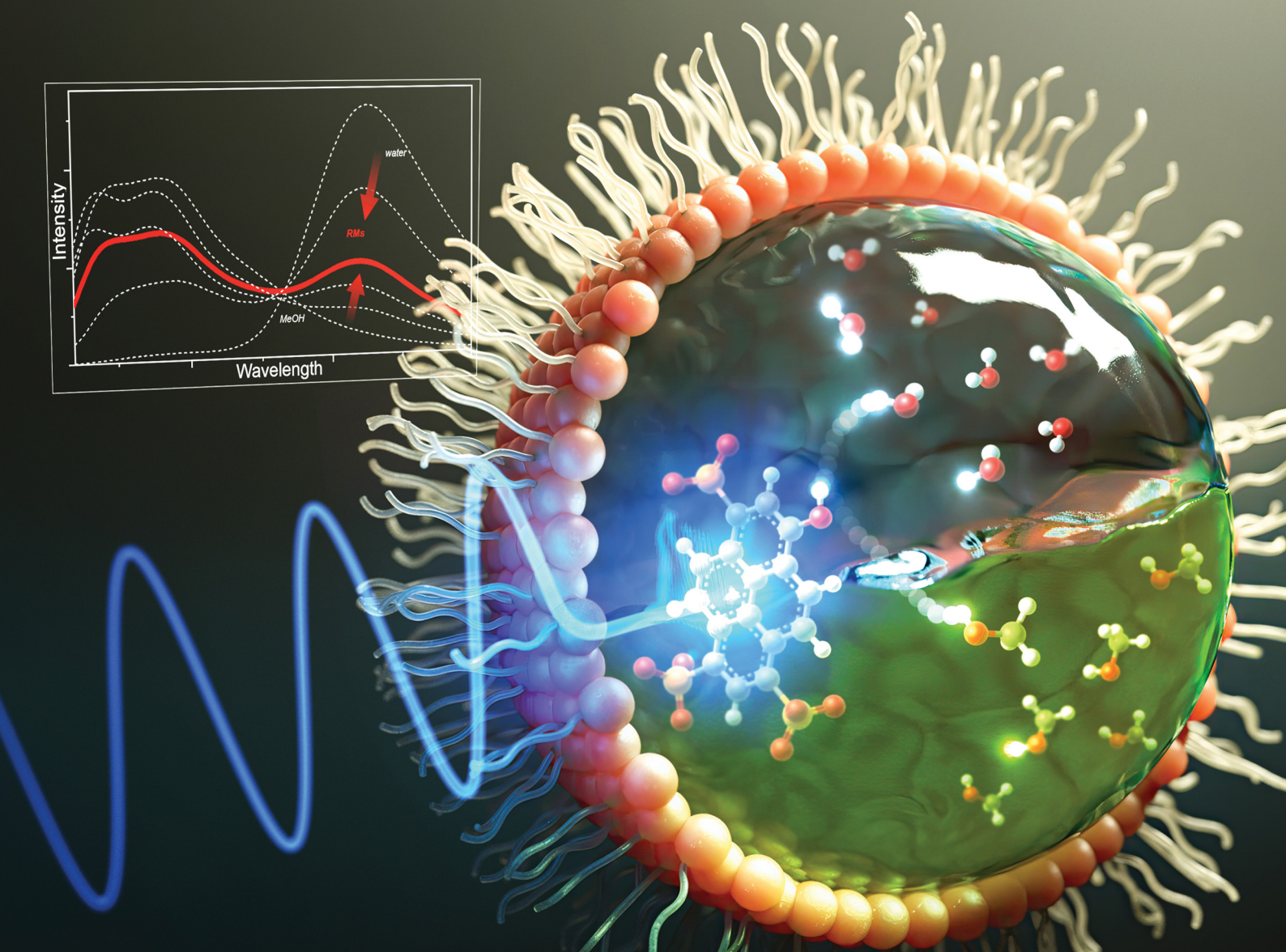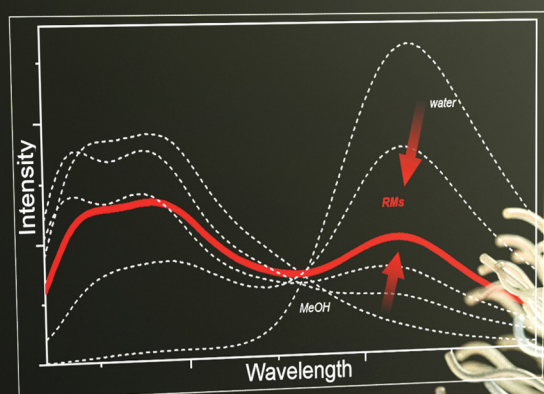
PAPER
Yoonsoo Pang *et al.*
Anomalous proton transfer of a photoacid HPTS in
nonaqueous reverse micelles

PCCP
Owner Societies

ROYAL SOCIETY
OF CHEMISTRY

Check for updates

Anomalous proton transfer of a photoacid HPTS in nonaqueous reverse micelles†

Taehyung Jang, Sebok Lee and Yoonsoo Pang (ID) *

The proton transfer reaction is one of the fundamental chemical reactions where the reaction dynamics strongly depend on solvent properties such as acidity or basicity. A photoacid 8-hydroxypyrene-1,3,6-trisulfonic acid (HPTS) shows a sharp decrease of pK_a (7.7 → 0.5) upon photoexcitation, and the excited-state proton transfer (ESPT) occurs with ultrafast time constants of 2.5 and 89 ps in bulk aqueous solution. However, the two-step proton transfers *via* the contact ion pair formation and the proton diffusion are strongly limited inside the nanopools of reverse micelles (RMs). The confinement in small RMs strongly impeded the proton transfer reactions. In this work, we report the ESPT of HPTS confined in *methanol-in-oil* RMs by steady-state and time-resolved electronic spectroscopy. Interestingly, HPTS shows substantial deprotonation in the excited state only in small RMs, while the ESPT of HPTS does not occur in bulk methanol solution due to the low basicity of aliphatic alcohols. The kinetic analysis of time-resolved fluorescence and transient absorption measurements will compare the proton transfer dynamics of HPTS in the *water-in-oil* and *methanol-in-oil* RMs. The ESPT of photoacids, especially in the nonaqueous RMs, can be crucial in understanding many important chemical reactions involving proton transfer in the confined environments of cells and membranes.

Introduction

Reverse micelles (RMs) are representative biomimetic structures where a monolayer of surfactant molecules separates the inner polar medium from the outer nonpolar medium.[1–3] Self-assembly of surfactant molecules and electrostatic interaction with the polar solvents are the driving forces for the RM formation. Thus, the size and structure of the RMs can be controlled by changing the shape of surfactant molecules or the molar ratio of surfactant to polar solvent. The RMs have been widely adopted in many photophysics and dynamics studies of small chromophores confined inside the polar core. The solvent nanopools inside the RMs are distinct from bulk in numerous solvent properties, including polarity, viscosity, and solvation.[4–9] Aerosol OT (AOT) and cetyltrimethylammonium bromide (CTAB) are among the most well-known surfactants with anionic and cationic head groups, respectively, to form RMs.[10,11] Nonionic surfactants, including Igepal, Brij, and Triton X, are also known to form RMs where the nanopools

may consist of a small number of polar solvents in nonpolar environments.[12–14] The surfactant charge is one of the critical parameters to determine the dynamic properties of polar solvents inside the RMs. The photophysical properties of chromophores, which strongly depend on the surfactant charges or polar environments inside the RMs, have been of interest in numerous experimental and theoretical studies.[7–9,15–21]

Chromophores confined in the RMs often face anomalously slower dynamics than bulk due to the decreased solvation originating from the small number of solvent molecules inside the nanopools.[4,16,22–24] Interfacial charges of the surfactant head groups are known to interfere with solvation dynamics or hydrogen bonding of polar solvents.[7,8,16,25] Chemical reaction dynamics in the RMs may be of great interest in many aspects since the RMs have been used for the synthetic vessels of certain nanoparticles, the model systems of numerous biochemical reactions in cell membranes.[26,27] Acid–base reactions in the confined environments of the RMs have been of great interest in understanding the proton transfer dynamics occurring in biological environments.[28–31] The determination of the acidity or basicity of a molecule inside the RMs is generally considered quite challenging, where a few indirect measurements of the local pH inside the RMs have been reported by visible and infrared absorption spectroscopy and NMR measurements of pH-sensitive chromophores.[32–38] The local pH of the water nanopools in the anionic (or nonionic) RMs was determined as neutral, and the buffer-like actions of

Department of Chemistry, Gwangju Institute of Science and Technology, 123 Cheomdangwagi-ro, Buk-gu, Gwangju 61005, Republic of Korea.
E-mail: ypang@gist.ac.kr

† Electronic supplementary information (ESI) available: Dynamic light scattering measurements; absorption and emission spectra in *water-in-oil* AOT RMs and Igepal CO-520 solution; ground- and excited-state pK_a measurements; fluorescence anisotropy in *methanol-in-oil* RMs; excited-state proton transfer (ESPT) dynamics in the RMs. See DOI: https://doi.org/10.1039/d3cp05710k

This journal is © the Owner Societies 2024

Phys. Chem. Chem. Phys., 2024, **26**, 11283–11294 | 11283

the amphiphilic surfactant molecules, such as charges on head groups and counterions have been attributed to the observed pH values.[34,37,38] Nonetheless, the acidity or basicity of methanol nanopools in the RMs have not been reported maybe due to the absence of appropriate indicator molecules in the methanol media.

8-Hydroxypyrene-1,3,6-trisulfonic trisodium salt (HPTS; pyranine) is one of the well-known photoacids, and the proton transfer dynamics of HPTS have been extensively investigated in many environments, including inside the RMs.[39–49] In bulk water, HPTS show a sharp decrease of the pK_a value (7.7 → 0.5) upon photoexcitation, and the excited-state proton transfer (ESPT) of HPTS occurs in two steps of contact ion pair formation ($\sim$3 ps) and proton dissociation ($\sim$90 ps).[40,50,51] The ESPT dynamics of HPTS have been reported in the anionic RMs of AOT and nonionic RMs of Igepal and Brij, where the proton transfer dynamics become slower (220–350 ps) compared to the bulk aqueous condition and also face substantial recombination (390 ps) between deprotonated HPTS and proton.[7,45] Similarly, much slower (50–250 ps) proton transfer dynamics of HPTS have been measured inside a live cell or cyclodextrin cavity, which shows a strong dependence of proton transfer dynamics on the local environments of heterogeneous or confined media.[52–55]

The proton transfer dynamics of photoacids in nonaqueous environments have been often reported.[41,56–60] Fayer and co-workers reported the proton transfer dynamics of HPTS in an aprotic solvent 1-methylimidazole, and the proton transfer of strong photoacids, including N-methyl-7-hydroxyquinolinium and pyranine derivatives, have been observed in alcoholic solvents. The proton transfer dynamics of photoacids generally depend on the excited-state acidity of the photoacid and the basicity of the solvent. However, the dependence of the proton transfer dynamics on the local environments, such as the confinement or the increased microviscosity inside small RMs, has not been investigated yet. Numerous interesting solvation dynamics and photophysics of organic chromophores have been studied in the nonaqueous nanopools of the RMs with methanol, acetonitrile, and dimethylsulfoxide.[8,20,24,61–66] Since the microscopic environments of RMs alter numerous solvent properties *via* confinement and hydrophobic/hydrophilic interactions with the surfactant head groups, abnormal changes in the proton transfer dynamics of a photoacid would be expected. It would be of great interest to find out whether the proton transfer dynamics in the nonaqueous RMs are similarly inhibited with the substantial increase of recombination rates as observed from the aqueous RM results, or whether the facilitated proton transfer dynamics in nonaqueous nanopools of RMs can be encountered in certain conditions. Several studies adopted the binary solvent mixtures of water–methanol or water–dimethylsulfoxide to investigate the effects on the proton transfer dynamics of HPTS.[41,44,67,68] The proton transfer dynamics in the binary mixtures decreased mainly due to the low basicity of aprotic solvents than water.

In this paper, the ESPT dynamics of HPTS in the RMs with methanol and water cores were investigated by steady-state and time-resolved absorption and emission spectroscopy. We observed anomalous ESPT of HPTS in small *methanol-in-oil* RMs, which is facilitated in the confined environment of RMs compared to the bulk. By comparing the micelle-size dependent proton transfer dynamics of HPTS in *methanol-in-oil* and *water-in-oil* RMs, we propose that the proton transfer dynamics in small RMs strongly depend on the abnormally slow solvation dynamics of the polar cores compared to the bulk rather than the solvent itself.

Experimental

Sample preparation

HPTS (TCI, Tokyo, Japan), Igepal CO-520 (average molecular weight of 441; Sigma-Aldrich, Milwaukee, WI, USA), and all the solvents were used without further purification. The RM samples were prepared by mixing a 0.6 M surfactant solution of Igepal CO-520 in a 1:1 mixture of cyclohexane and n-hexane with a 1×10^{-3} M HPTS solution in water or methanol. When required, additional water or methanol was added for the specific molar ratio, ω = [water or methanol]/[Igepal CO-520] between the polar solvent and surfactant. The final concentration of HPTS in all RM samples was kept as 1×10^{-5} M, where a micelle containing two or more HPTS molecules would not exist. The phosphate buffer solutions (pH 4.0 and 10.0, Duksan, Seoul, Korea) were used in the sample preparation for the absorption and emission measurements of neutral and deprotonated species of HPTS in water/Igepal CO-520/cyclohexane-n-hexane RMs.

Dynamic light scattering

The formation of *water-in-oil* and *methanol-in-oil* RMs with the surfactant Igepal CO-520 was confirmed by the DLS measurements with a particle size analyzer (Zetasizer Ultra; Malvern Panalytical Ltd., Malvern, UK) with a 632.8 nm laser, and the viscosity measurements at 25 °C with a rotational viscometer (DV-II + Pro; AMETEK Brookfield, Middleboro, MA, USA). All the RMs samples were filtered through a 0.2 μm syringe filter before the DLS and viscosity measurements. As shown in Fig. S1 and S2 (ESI†), the hydrodynamics diameters of the *water-in-oil* and *methanol-in-oil* RMs were determined as 5.1–8.9 nm (with the water to surfactant ratio ω = 1–15) and 3.8–4.3 nm (with the methanol to surfactant ratio ω = 1–5), respectively. The micelle formation of the *methanol-in-oil* RMs appears unstable with ω = 8 or 15, where the microemulsions with much higher inhomogeneity in the hydrodynamic diameter were observed.[61,69]

Steady-state and time-resolved spectral measurements

The steady-state absorption spectra were measured in a commercial spectrophotometer (Mega-900; Scinco, Seoul, Korea), and the emission spectra and kinetics were obtained using a home-built TCSPC setup.[8,70] The excitation laser at 405 nm with a pulse energy of $\sim$18 pJ and pulse duration of $\sim$70 ps at 10 MHz was used, and the IRF of $\sim$150 ps in FWHM was obtained with a photomultiplier tube detector (PMA 192; PicoQuant GmbH, Berlin, Germany) and a TCSPC module

11284 | *Phys. Chem. Chem. Phys.*, 2024, **26**, 11283–11294

This journal is © the Owner Societies 2024

(PicoHarp 300; PicoQuant GmbH). The spectral resolution of ~ 2 nm was used in most of the spectral and kinetic measurements. To minimize the contribution from the reorientational dynamics of samples in the fluorescence lifetime measurements, the emission from the sample was collected at a magic angle.[71]

The details of the femtosecond transient absorption setup based on 1 kHz Ti:sapphire regenerative amplifier (Libra-USP-HE; Coherent, Santa Clara, CA, USA) were described elsewhere.[70,72] The actinic pump at 403 nm was generated by second-harmonic generation in a BBO crystal (0.1 mm thick; A-Star Photonics, Fuzhou, China) and compressed by a chirped mirror pairs (-30 ± 10 fs^2 group delay dispersion; Layertec GmbH, Mellingen, Germany). The white-light probe pulse prepared by super-continuum generation in a sapphire crystal was measured in a CCD spectrometer (QE65Pro; Ocean Optics, Largo, FL, USA), and an IRF of ~ 50 fs in FWHM was obtained between the actinic pump and probe pulses in the optical Kerr effect measurements.

Data analysis

The ESPT dynamics of HPTS from the transient absorption and TCSPC measurements were analyzed by a multi-exponential fit convoluted with the IRF in the software packages of Glotaran and Fluofit (PicoQuant GmbH).[73]

Results

Steady-state absorption and emission spectra

Fig. 1 shows the steady-state absorption and emission spectra of HPTS in water/Igepal CO-520/cyclohexane-*n*-hexane RMs and bulk water. The absorption spectra of HPTS in bulk water are strongly pH-dependent: the absorption bands at 370 and 405 nm represent the neutral species, while the red-shifted band at 455 nm denotes the deprotonated species. The pK_a of HPTS in aqueous solution is reported as 7.7.[50] The absorption spectra of HPTS in the *water-in-oil* RMs were quite similar to that of neutral HPTS in bulk. As the micelle size decreases ($\omega = 15 \rightarrow 1$), partial deprotonation is observed with slight decreases in the neutral bands and small increases in the deprotonated band. On the other hand, HPTS in the *water-in-oil* RMs with anionic surfactants (AOT) show substantial deprotonation due to the electrostatic interactions with the sulfonate head group of AOT (refer to the absorption and emission spectra in Fig. S3, ESI†).[74,75] Moreover, the emission intensity of HPTS in the small *water-in-oil* AOT RMs ($\omega = 1, 3$) is largely quenched due to the electrostatic interactions with the surfactant head groups. Thus, the anionic AOT RMs are considered inadequate for investigating the ESPT and resulting photophysical properties of HPTS. This work mainly focuses on the experimental results with the nonionic Igepal RMs. Nonetheless, partial deprotonation of HPTS observed from the absorption measurements in the *water-in-oil* RMs (Fig. 1(a)) may be related to the slower solvation dynamics of water in the small RMs rather than the electrostatic interactions with the surfactant head groups.[75]
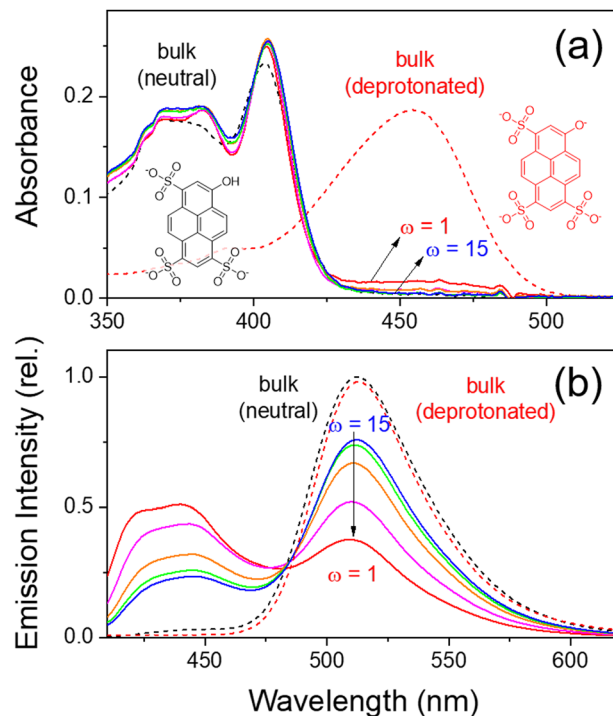

Fig. 1 (a) Steady-state absorption and (b) emission spectra of HPTS in bulk water and *water-in-oil* Igepal RMs of $\omega = 1, 3, 5, 8$, and 15. Absorption and emission spectra of the neutral and deprotonated species of HPTS obtained in bulk water at neutral and basic (pH = 10) conditions, respectively, were displayed as dotted lines for comparison, along with the molecular structures of both species. The emission spectra were normalized with respect to the absorbance of each sample at the excitation wavelength of 405 nm.

HPTS shows a substantial decrease of pK_a down to ~ 0.5 in the excited state.[41,50,76] The emission band at 510 nm, commonly observed with the neutral and basic bulk aqueous solutions (Fig. 1(b)), represents the emission from the deprotonated species of HPTS.[50] On the other hand, HPTS in the *water-in-oil* RMs shows dual emission bands at 440 (neutral) and 510 nm (deprotonated).[7,45,75] The relative intensities of the deprotonated (*vs.* neutral) emission bands of HPTS largely decrease with the decreasing micelle size, which shows that the deprotonation of HPTS becomes limited in the RMs with a strong dependence on the micelle size. Fayer and co-workers investigated the intermolecular proton transfer dynamics of HPTS in the nonionic *water-in-oil* RMs, where the recombination dynamics between the deprotonated HPTS and proton was strongly facilitated with the attenuated deprotonation in the confined space of the small RMs.[7] Based on the absorption and emission measurements, it is concluded that HPTS exists mainly in a neutral species in the *water-in-oil* RMs, and the deprotonation of HPTS in the excited state appears strongly hampered, especially in the small RMs.

The steady-state absorption and emission spectra of HPTS in methanol/Igepal CO-520/cyclohexane-*n*-hexane RMs and bulk methanol are shown in Fig. 2. The absorption spectrum of HPTS in bulk methanol appears quite similar to that in bulk water except for the better-developed vibronic patterns with the
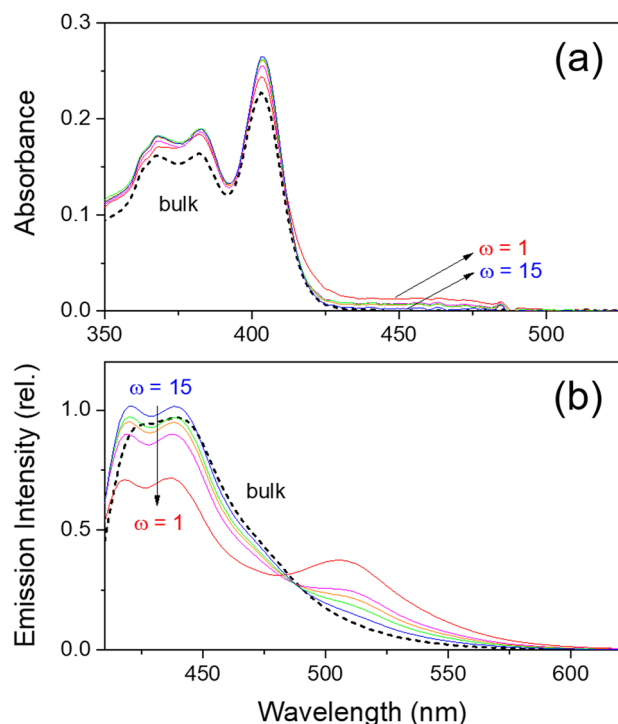
Fig. 2 (a) Steady-state absorption and (b) emission spectra of HPTS in bulk methanol and *methanol-in-oil* Igepal RMs of ω = 1, 3, 5, 8, and 15. Absorption and emission spectra of HPTS obtained in bulk methanol were displayed as dotted lines for comparison. The emission spectra were normalized with respect to the absorbance of each sample at the excitation wavelength of 405 nm.

absorption maxima at 403, 382, and 368 nm. The absorption spectra of HPTS in the *methanol-in-oil* RMs are also quite similar to the bulk spectrum except for a small portion of the deprotonated absorption band (at 430–480 nm) in the small RMs. In absorption measurements, HPTS shows almost no difference between the *methanol-in-oil* and *water-in-oil* RMs. Therefore, it is considered that HPTS exists in the neutral species in the RMs regardless of water or methanol core, except for the small micelles where a partial deprotonation may occur.

The emission spectrum of HPTS in bulk methanol (Fig. 2(b)) mainly shows a neutral emission band broadly centered at 430–440 nm, representing that HPTS in methanol solution does not deprotonate in the excited states. However, HPTS in the *methanol-in-oil* RMs shows dual emission bands at 421/439 nm (neutral; similar to bulk emission) and 506 nm (deprotonated). The deprotonated emission intensity increases with the decrease of the micelle size while the neutral emission intensities decrease. Surprisingly, the photon-induced deprotonation of HPTS seems to be facilitated in the small (ω = 1–5) *methanol-in-oil* RMs, which is opposite to the ESPT observed in the small *water-in-oil* RMs. Interestingly, the emission spectra of HPTS in the small (ω = 1) RMs shown in Fig. 1(b) and 2(b) are very similar regardless of the difference in the polar core (waver *vs.* methanol). The deprotonation of HPTS in the *methanol-in-oil* RMs does not originate from the acid–base reactions with the surfactant molecules. As shown in Fig. S4 (ESI†), the emission

spectra of HPTS in Igepal/methanol mixture and Igepal only show only the neutral emission bands while the spectrum in small *methanol-in-oil* RMs shows substantial deprotonation. The emission of HPTS shows strong quenching in Igepal CO-520 only. Thus, HPTS is considered to exist mainly inside the RMs and the penetration into the tails of the surfactant is considered negligible.

The pK_a values of HPTS in methanol were determined in the ground and excited states using the absorption and emission changes for the protonated and deprotonated bands. As shown in Fig. S6 (ESI†), the pK_a values of HPTS in methanol were determined as 11.3 (ground state from absorption changes) and 11.8 (excited state from emission changes). A substantial increase of the ground state pK_a values in methanol compared to the aqueous solution has generally been observed for small organic molecules of phenols and carboxylic acids.[77] The excited-state pK_a^* of HPTS was estimated as $\sim$4 in the extrapolation of the proton transfer rate (k_{PT}) values of the water–methanol binary mixtures,[41,44,78] which appears much lower than our results from the emission measurements.

HPTS is classified into a weak-intermediate strength photoacid with positive excited-state pK_a^* values in water. In methanol solution, the k_{PT} of HPTS is estimated to decrease by about 4 orders of magnitude compared to the aqueous solution.[44] The deprotonation of HPTS was not observed even in the excited state in bulk methanol solution, which can be understood as the largely decreased autoprotolysis constant of methanol, $K_{MeOH} = 2.0 \times 10^{-17}$ compared to that of water, $K_W = 1.0 \times 10^{-14}$,[79] or its low basicity. However, the ESPT of HPTS was observed from the emission measurements in the small *methanol-in-oil* RMs, where the details of proton transfer mechanism can further be explored by time-resolved spectroscopy.

Time-resolved fluorescence measurements of HPTS in the RMs

Time-resolved fluorescence spectra and kinetics of HPTS in *water-in-oil* RMs and the bulk aqueous solution obtained with the 405 nm excitation are shown in Fig. 3. In the area-normalized fluorescence spectrum of each sample, called time-resolved area-normalized emission spectrum (TRANES), the kinetically-coupled emissive species are evidenced by the presence of an isosbestic point.[75,80] The neutral (440 nm) and deprotonated (512 nm) emission bands of HPTS in all the RMs and bulk aqueous solution represent an isoemissive point at 492 nm, which shows that the dissociation of a proton kinetically connects two emission bands of HPTS.

The intensity ratio of the deprotonated emission band to the neutral band at a time delay of 10 ns, for example, clearly shows that the deprotonation of HPTS in the *water-in-oil* RMs becomes slower with the decrease of the micelle size. The deprotonation of HPTS appears to be completed in 10 ns in the large (ω = 15) RMs, while the deprotonation completes in 1–2 ns in bulk water. Moreover, about one-third of HPTS remain protonated in the excited state at a long delay of 10 ns in the small (ω = 1) RMs. It is understood that the diffusion of the detached proton can be limited in the confined space of the RMs. Thus, the
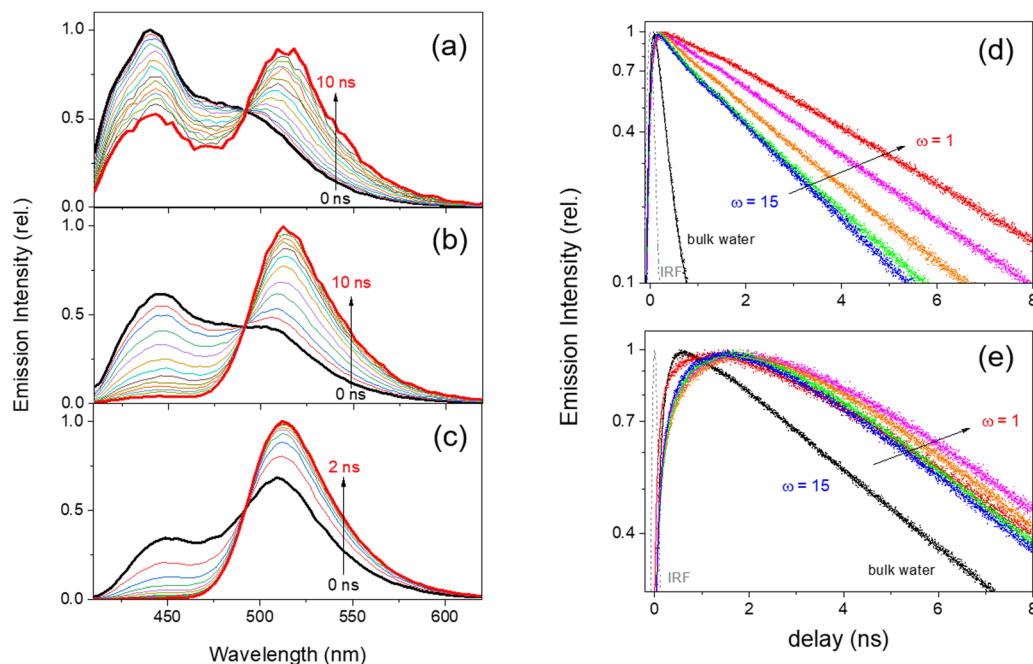
11286 | *Phys. Chem. Chem. Phys.*, 2024, **26**, 11283–11294

This journal is © the Owner Societies 2024

Fig. 3 Time-resolved area-normalized emission spectra (TRANES) of HPTS in *water-in-oil* Igepal RMs of (a) ω = 1 and (b) ω = 15, and (c) bulk water; emission kinetics of HPTS in *water-in-oil* RMs probed at (d) 440 (neutral) and (e) 510 nm (deprotonated). The 405 nm excitation was used for all the emission measurements, and the instrumental response function (IRF) of the fluorescence measurements was also displayed.

recombination rate of proton and deprotonated HPTS increases in the small RMs.[7,45,75] The deprotonation dynamics of HPTS were obtained by the multi-exponential analysis of the time-resolved fluorescence results.[7,51,81,82] Table 1 summarizes the emission kinetics for the deprotonated species of HPTS in the *water-in-oil* RMs. Two fast-rising components τ_1 and τ_2 in the emission kinetics of the deprotonated species may represent the formation of the contact ion pair and the dissociation of the proton, while the slowest component τ_3 represents the lifetime of the deprotonated species.[7,51,81,82] The emission kinetics for the neutral species of HPTS also show matching decay components as τ_1 and τ_2, which shows that the decrease of the neutral emission and deprotonated emission bands are kinetically coupled. As shown in Fig. 3(d), the deprotonation dynamics of HPTS, represented by τ_1 and τ_2 increase with the decrease of

the micelle size in the *water-in-oil* RMs. It is noted that the lifetime of the deprotonated species τ_3 in the RMs is almost invariant from the bulk values.

Time-resolved fluorescence spectra and kinetics of HPTS in *methanol-in-oil* RMs and bulk methanol solution obtained with the 405 nm excitation are shown in Fig. 4. The deprotonated emission band (510 nm) of HPTS has been observed in the *methanol-in-oil* RMs, while only the neutral emission bands (415–440 nm) appear in bulk methanol even in the excited state. The isoemissive points appearing at 500–505 nm (ω = 1) and 480 nm (ω = 8) represent that the neutral and deprotonated emission bands of HPTS in the *methanol-in-oil* RMs are kinetically coupled to the proton dissociation. However, the deprotonation dynamics in the *methanol-in-oil* RMs may be more complicated than those in the *water-in-oil* RMs since the

Table 1 Emission kinetics for the deprotonated HPTS in *water-in-oil* and *methanol-in-oil* RMs

	a_1	τ_1 (ns)	a_2	τ_2 (ns)	a_3	τ_3 (ns)
Water-in-oil RMs and bulk aqueous solution (probed at 510 nm)						
ω = 1	−0.07	0.27 ± 0.08	−0.30	2.24 ± 0.05	0.63	5.23 ± 0.02
ω = 3	−0.08	0.28 ± 0.05	−0.36	2.14 ± 0.03	0.56	5.10 ± 0.02
ω = 5	−0.08	0.27 ± 0.04	−0.35	1.64 ± 0.03	0.57	5.14 ± 0.02
ω = 8	−0.11	0.23 ± 0.03	−0.32	1.32 ± 0.03	0.57	5.16 ± 0.02
ω = 15	−0.12	0.17 ± 0.03	−0.29	0.79 ± 0.03	0.59	5.19 ± 0.02
Bulk water	−0.57	0.13 ± 0.00	−0.02	0.69 ± 0.04	0.41	5.36 ± 0.01
Methanol-in-oil RMs and bulk methanol solution (probed at 510 nm)						
ω = 1	−0.09	0.35 ± 0.09	−0.24	1.98 ± 0.07	0.67	5.07 ± 0.02
ω = 3	−0.11	0.56 ± 0.10	−0.25	2.05 ± 0.08	0.64	5.03 ± 0.03
ω = 5	−0.16	0.73 ± 0.08	−0.20	2.41 ± 0.09	0.64	4.98 ± 0.02
ω = 8	−0.19	0.71 ± 0.08	−0.17	2.65 ± 0.08	0.64	4.94 ± 0.03
ω = 15	−0.24	0.59 ± 0.08	−0.06	2.98 ± 0.14	0.70	4.84 ± 0.03
Bulk methanol	−0.25	0.17 ± 0.04	−0.02	2.91 ± 0.12	0.73	3.86 ± 0.03

This journal is © the Owner Societies 2024

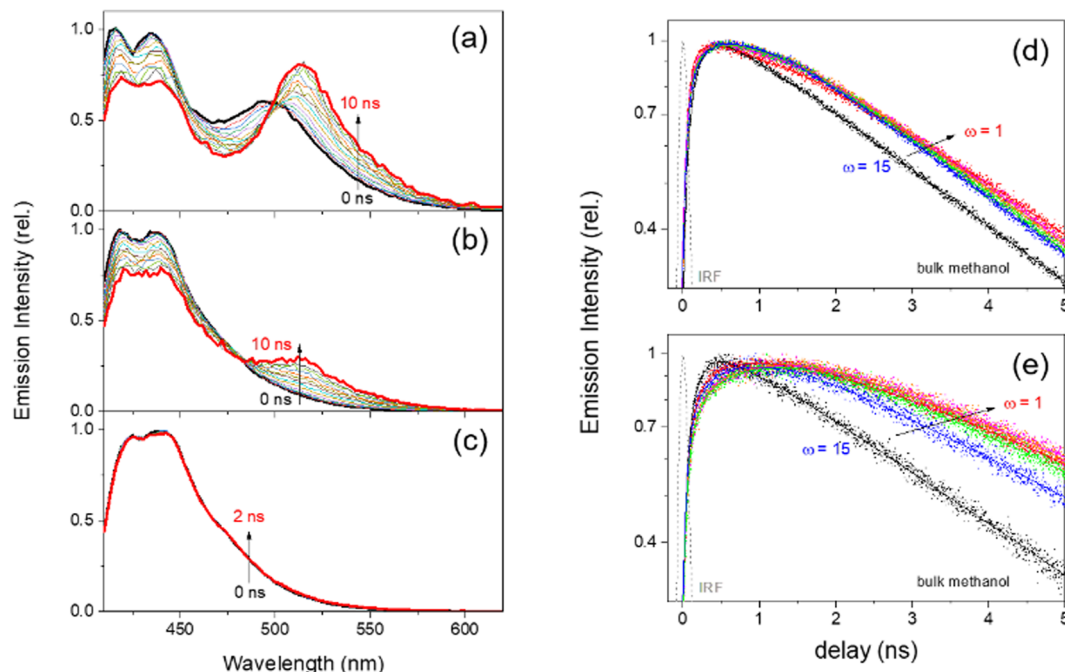*Phys. Chem. Chem. Phys.*, 2024, **26**, 11283–11294 | **11287**

Fig. 4 Time-resolved area-normalized emission spectra (TRANES) of HPTS in *methanol-in-oil* Igepal RMs of (a) $\omega = 1$ and (b) $\omega = 8$, and (c) bulk methanol; emission kinetics of HPTS in *methanol-in-oil* RMs probed at (d) 440 (neutral) and (e) 510 nm (deprotonated). The 405 nm excitation was used for all the emission measurements, and the instrumental response function (IRF) of the fluorescence measurements was also displayed.

appearance of the isosbetic points in TRANES is less clear with slight spectral evolutions. The emission kinetics of HPTS in *methanol-in-oil* RMs for the deprotonated species were similarly analyzed by the multi-exponential fits, and the results were summarized together with the results of the *water-in-oil* RMs in Table 1. Two rising components in the deprotonated (510 nm) emission kinetics represent the deprotonation dynamics of HPTS in *methanol-in-oil* RMs, which becomes slightly faster in the small RMs. HPTS in large ($\omega = 8$) RMs show two-step deprotonation dynamics of $\tau_1 = 0.71$ and $\tau_2 = 2.65$ ns, while these dynamics become slightly faster (0.35 and 1.98 ns) in small ($\omega = 1$) RMs. The lifetime of the deprotonated species τ_3 of HPTS becomes slower in the *methanol-in-oil* RMs from the bulk with a minor dependence on the micelle size. The deprotonation dynamics of HPTS in the *methanol-in-oil* RMs were only partly separable from the kinetics for the neutral (440 nm) emission bands; $\tau_2 = 2.8$ ns for the medium or large RMs. The rotational relaxation dynamics with faster time constants of 0.56–1.4 ns would complicate the kinetic analysis of the neutral emission bands.[44,51,83,84]

The location of HPTS molecules in aqueous RMs depends on the surfactants, especially the charges on the head groups.[7,47] In anionic (AOT) RMs, the probe shows less restricted rotations due to repulsion from anionic head groups. Large semi-cone angles ($\theta = 59$–$60°$) of wobbling motions from anisotropy measurements represent free rotation of probe molecules inside the anionic RMs.[7] Conversely, much smaller semi-cone angles ($\theta = 13$–$23°$) were observed in cationic (BHDC) RMs representing that the probe molecule is strongly attached to the interface of surfactant head groups.[47] In case of nonionic

(Igepal) RMs, slightly smaller semi-cone angle ($\theta = 42$–$45°$; but much larger than the cationic RMs) was obtained representing that the probe molecules mainly exist inside the RMs with an increased interaction with the micelle interfaces compared to the anionic RMs. The rotational dynamics for the neutral species of HPTS were confirmed by fluorescence anisotropy measurements (refer to Fig. S7, ESI†), where similar semi-cone angles ($\theta = 45$–$48°$) as those in aqueous nonionic RMs was obtained and the wobbling time (τ_w) also showed micelle size dependence. Therefore, HPTS molecules are considered to exist inside the *methanol-in-oil* RMs with possible interactions with the surfactant head groups.

Transient absorption measurements of HPTS in the RMs

From the time-resolved fluorescence measurements, we retrieved micelle-size-dependent two-step proton transfer dynamics of HPTS in both RMs: 0.17–0.27 and 0.79–2.24 ns for *water-in-oil* RMs and 0.59–0.35 and 2.98–1.98 ns for *methanol-in-oil* RMs (in the order of decreasing micelle size). The ESPT dynamics of HPTS in *water-in-oil* RMs are compatible with previously reported values with nonionic surfactants of Igepal and Brij.[7,45] However, the fast kinetic components for the ESPT of HPTS, including the results of the bulk aqueous solution, are close to time resolution (~ 150 ps) of fluorescence measurements, so further confirmation by time-resolved electronic spectroscopy with higher temporal resolution would be needed.

Femtosecond transient absorption spectra of HPTS in the RMs and bulk solutions of water and methanol obtained with the 403 nm excitation are shown in Fig. 5. The deprotonation of
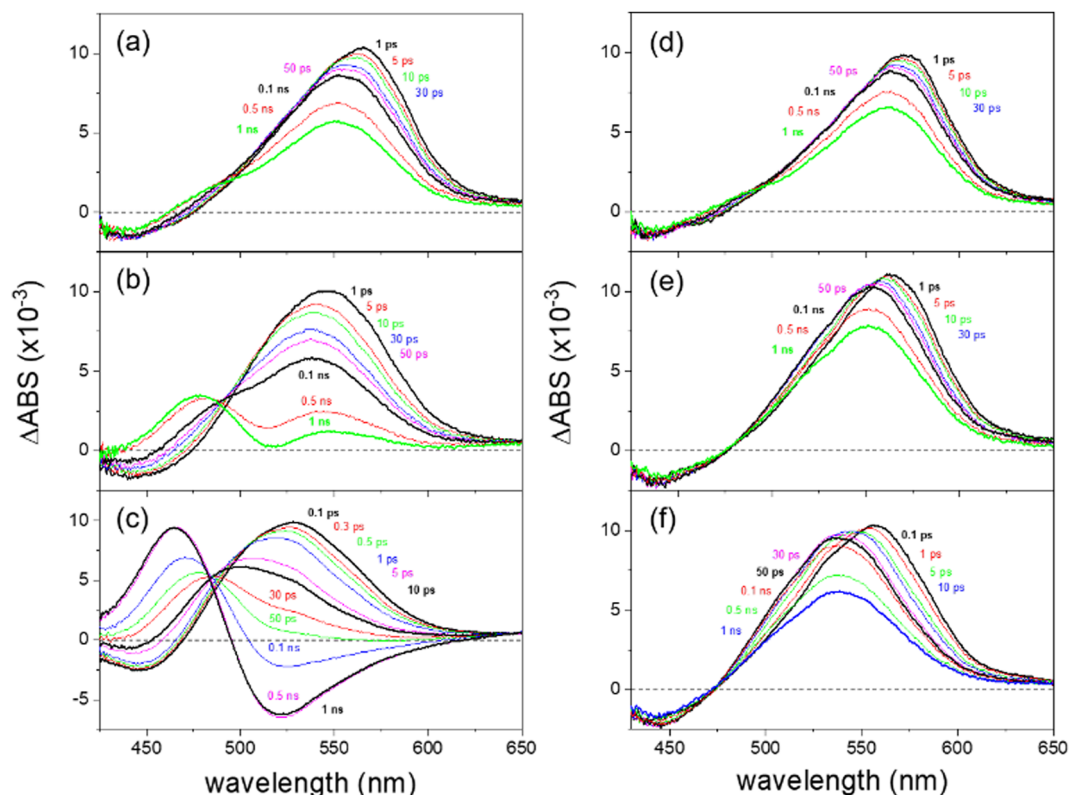
Fig. 5 Transient absorption spectra of HPTS in *water-in-oil* RMs of (a) ω = 1 and (b) ω = 15, and (c) bulk water; transient absorption spectra of HPTS in *methanol-in-oil* RMs of (d) ω = 1 and (e) ω = 15, and (f) bulk methanol. The 403 nm excitation was used for all the transient absorption measurements.

HPTS is determined from the excited-state absorption (ESA) and stimulated emission (SE) bands of neutral (protonated) and deprotonated species. The ESA band at 525–530 nm and a weak SE band at 450 nm appearing at early time delays represent the neutral species of HPTS in the bulk aqueous solution (Fig. 5(c)), while another ESA band at 470 nm and SE band at 520 nm appearing at 0.5–1 ns time delay represent the deprotonated species of HPTS. Similarly, the ESA and SE bands of neutral HPTS in the bulk methanol solution (Fig. 5(f)) appear at 535–555 nm and 455 nm, respectively. The transient absorption spectra of HPTS in the bulk methanol solution show no significant spectral changes except for the solvation dynamics in 10–20 ps, which shows that the deprotonation of HPTS does not occur in methanol.

In all the RM samples with water or methanol core, the spectral features of the deprotonated species are not separately observed except in the large (ω = 15) *water-in-oil* RMs. The ESA bands of the neutral species appear at 539–566 nm in the *water-in-oil* RMs and 552–572 nm in the *methanol-in-oil* RMs, and the weak SE bands of the neutral species appear commonly at 440–455 nm. The ESA bands of the deprotonated species appear at 480 nm in the large (ω = 15) *water-in-oil* RMs, while the SE bands appear mixed with the positive ESA bands of the remaining neutral species. The SE bands of deprotonated species of HPTS in the small (ω = 1) *water-in-oil* and *methanol-in-oil* RMs appear as the partial decreases in the ESA bands of the neutral species at 505–510 nm in the long time delay of 1 ns.

The transient absorption kinetics for the neutral (protonated) and deprotonated species of HPTS in the *water-in-oil*

RMs and the bulk aqueous solution were obtained from a global fit with a sequential model.[73] Fig. 6 shows the evolution-associated difference spectra (EADS) obtained from the global analysis, representing each kinetic component's absorption and emission spectral features. The fastest kinetic components represent the solvation dynamics, similarly assigned in previous reports.[52–55] The spectral evolution in the ESA bands of the neutral species shows apparent blue-shifts for the EADS of the second kinetic components compared to those of the fastest components, which were similarly obtained from the dynamics Stokes' shifts analysis (refer to Fig. S8 in the ESI†). Ultrafast (0.44 ps) solvation dynamics in the bulk aqueous solution become slower in the *water-in-oil* RMs (1.6 ps for ω = 15 and 3.7 ps for ω = 1) with the decreased solvent interactions in the small RMs.[85,86] The deprotonation of HPTS shows the biexponential decays of 2.5 and 89 ps in the bulk aqueous solution, which has been previously interpreted as the formation of contact ion pair and the diffusion of proton.[40,50,87] The deprotonation of HPTS becomes slower in the *water-in-oil* RMs with an apparent micelle-size dependence: 29 and 480 ps for large (ω = 15) RMs and 96 ps and 2.24 ns for small (ω = 1) RMs. The deprotonation dynamics of HPTS in the *water-in-oil* RMs and bulk aqueous solutions are much faster than the time resolution ($\sim$150 ps) of time-resolved fluorescence measurements. Thus, the kinetic components retrieved from the transient absorption measurements should be used for the further ESPT dynamics analysis of HPTS in the *water-in-oil* RMs and bulk aqueous solution.
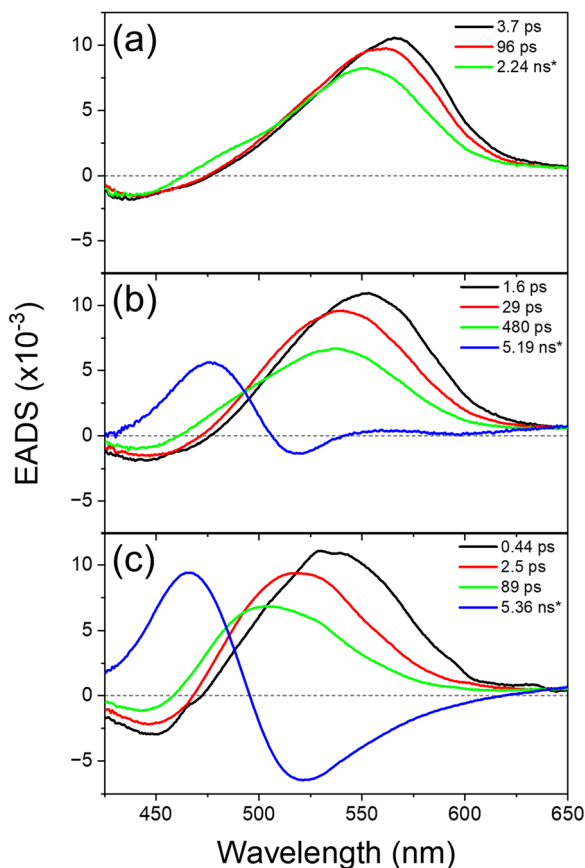
Fig. 6 Evolution–associated difference spectra (EADS) of HPTS obtained from transient absorption results in (a) $\omega = 1$, (b) $\omega = 15$ *water-in-oil* RMs, and (c) bulk water. The fastest components represent the solvation dynamics; the next two are the proton transfer dynamics. The slowest components shown in $\omega = 15$ RMs and bulk water represent the deprotonated species of HPTS (population dynamics).

Similarly, the transient absorption kinetics of HPTS in the *methanol-in-oil* RMs and bulk methanol solution were analyzed by the global multi-exponential fits for the ESA and SE bands of the neutral (protonated) and deprotonated species. However, the ultra-fast solvation dynamics of 0.49 (bulk), 2.3 ($\omega = 15$ RMs), and 2.6 ps ($\omega = 1$ RMs) were only separately obtained from the slow (2.6–3.0 ns) population dynamics of the neutral species of HPTS. Since the kinetic data up to 1 ns time delay were only measured in transient absorption, the population dynamics from the time-resolved fluorescence measurements (3.7–3.8 ns for the decay of the neutral emission bands) were considered more accurate. The ESPT dynamics of HPTS in the *water-in-oil* and *methanol-in-oil* RMs will be further described in the next section by combining the kinetic results obtained from transient absorption (for *water-in-oil* RMs) and time-resolved fluorescence (for *methanol-in-oil* RMs) measurements.

Discussion

The ESPT of a photoacid HPTS in the *water-in-oil* and *methanol-in-oil* RMs is known to occur in two steps of contact ion pair

$([H^+ \cdots A^-]^*)$ formation and proton dissociation, similarly as in bulk water.[40,87,88] As shown in Scheme 1, the rate constants for proton transfer (k_{PT}), recombination (k_{rec}), and dissociation (k_{diss}) of a proton can be determined from the kinetic results of the neutral (HA*) or deprotonated (A^{-*}) species of a photoacid HPTS which show multi-exponential decay/growth components in time-resolved fluorescence and absorption measurements. This model has also been adopted for the proton transfer of HPTS in heterogeneous systems such as cyclodextrin, niosome, and live cells.[52–55]

The evolution of excited-state species of HPTS, HA*, $[H^+ \cdots A^-]^*$, and A^{-*} are described by a set of coupled differential equations with the rate constants of k_{PT}, k_{rec}, k_{diss}, k_{pr}, k_{HA}, and k_{A^-},

$$\frac{d}{dt}\begin{pmatrix} [HA]^* \\ [H^+ \cdots A^-]^* \\ [A^-]^* \end{pmatrix} = \begin{pmatrix} -X & k_{rec} & 0 \\ k_{PT} & -Y & k_{pr}[H^+]_w \\ 0 & k_{diss} & -Z \end{pmatrix}\begin{pmatrix} [HA]^* \\ [H^+ \cdots A^-]^* \\ [A^-]^* \end{pmatrix}$$

(1)

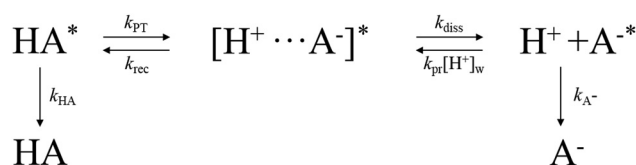where X, Y, and Z represent the sums of the following rate constants.

$$X = k_{PT} + k_{HA} \tag{2}$$

$$Y = k_{rec} + k_{diss} + k_{A^-} \tag{3}$$

$$Z = k_{pr}[H^+]_w + k_{A^-} \approx k_{A^-} \tag{4}$$

Since the protonation rate of A^{-*} depends on the concentration of the proton $[H^+]_w$, the protonation rate term $k_{pr}[H^+]_w$ can be neglected in most cases except in acidic conditions (pH < 3).[88] The rate constants for the ESPT of HPTS, k_{PT}, k_{rec}, and k_{diss} are evaluated from the amplitudes and decay constants of the excited-state species HA* or A^{-*} obtained from the time-resolved fluorescence and transient absorption measurements by the solutions of eqn (1), which is described in detail in the ESI.†

Table 2 lists the excited-state decay parameters HPTS in the RMs and the bulk aqueous solution obtained from time-resolved fluorescence and transient absorption measurements in addition to the proton transfer rate constants of HPTS determined from the solutions of eqn (1). The deprotonation dynamics of HPTS in bulk aqueous solution have been numerously reported, where the proton transfer (k_{PT}) and recombination (k_{rec}) rate constants show little variations depending on the amplitudes of the decay functions.[40,51,82] We obtained the values of $k_{PT} = 1.3 \times 10^{11}$ s^{-1} and $k_{rec} = 2.5 \times 10^{11}$ s^{-1} from transient absorption results, which is compatible with the previous reports.

$$HA^* \underset{k_{rec}}{\overset{k_{PT}}{\rightleftarrows}} [H^+ \cdots A^-]^* \underset{k_{pr}[H^+]_w}{\overset{k_{diss}}{\rightleftarrows}} H^+ + A^{-*}$$

$$\downarrow k_{HA} \qquad\qquad\qquad\qquad\qquad\qquad\qquad \downarrow k_{A^-}$$

$$HA \qquad\qquad\qquad\qquad\qquad\qquad\qquad\qquad A^-$$

Scheme 1 The excited-state proton transfer (ESPT) of a photoacid HA.

Table 2 Deprotonation dynamics of HPTS in the *water-in-oil* and *methanol-in-oil* RMs and in bulk solutions of water and methanol

	a_1	τ_1 (ps)	a_2	τ_2 (ns)	$\tau_{HA}{}^a$ (ns)	$\tau_f{}^a$ (ns)	k_{PT} (s^{-1})	k_{rec} (s^{-1})	k_{diss} (s^{-1})
Water[b]									
RMs ($\omega = 1$)	0.23	96 ± 1	0.65	2.24 ± 0.05^c	3.71	5.23	2.9×10^9	6.2×10^9	1.3×10^9
RMs ($\omega = 15$)	0.24	28.5 ± 0.4	0.55	0.48 ± 0.01	2.40	5.19	1.2×10^{10}	1.9×10^{10}	5.8×10^9
Bulk	0.21	2.5 ± 0.0	0.49	0.089 ± 0.001	2.49	5.36	1.3×10^{11}	2.5×10^{11}	3.5×10^{10}
Methanol[b]									
RMs ($\omega = 1$)	0.09	350 ± 90	0.24	1.98 ± 0.07	3.78	5.07	9.1×10^8	9.6×10^8	1.0×10^9
RMs ($\omega = 3$)	0.11	560 ± 100	0.25	2.05 ± 0.08	3.67	5.03	6.3×10^8	4.1×10^8	7.7×10^8
RMs ($\omega = 5$)	0.16	730 ± 80	0.20	2.41 ± 0.09	3.76	4.98	5.8×10^8	2.7×10^8	4.7×10^8
RMs ($\omega = 8$)	0.19	710 ± 80	0.17	2.65 ± 0.08	3.82	4.94	6.6×10^8	2.9×10^8	3.7×10^8

[a] τ_{HA} and τ_f represent the emission lifetimes of the neutral and deprotonated species of HPTS, separately measured from time-resolved fluorescence measurements. [b] Deprotonation dynamics of HPTS in *water-in-oil* RMs and aqueous solution were obtained from transient absorption measurements, while the dynamics in *methanol-in-oil* RMs were from time-resolved fluorescence measurements. [c] τ_2 obtained from time-resolved fluorescence measurements was used in the global fit.

Fayer and co-workers reported the deprotonation dynamics of HPTS in the AOT and Igepal RMs with the water core by time-resolved fluorescence measurements.[7,81] The largely decreased deprotonation dynamics of photoacids in the RMs are attributed to the confinement effects of nanoscopic water pools, which include the abnormally weaker solvation and smaller dielectric constant than bulk.[54,89] We update the deprotonation dynamics of HPTS in the *water-in-oil* Igepal RMs with the transient absorption results, where the much faster time constants (30–100 ps) for the deprotonation in the RMs were observed compared to the value from picosecond fluorescence measurements. The resulting values of k_{PT} (1.2×10^{10} s^{-1} for $\omega = 15$ and 2.9×10^9 s^{-1} for $\omega = 1$), which decrease with the micelle size decrease, appear consistent with the previous results ($1.0 \times 10^{10} \rightarrow 3.57 \times 10^9$ s^{-1} with $\omega = 20 \rightarrow 3$) by time-resolved fluorescence.[7]

The recombination rate constant (k_{rec}) values of HPTS in the *water-in-oil* RMs were determined as 1.9×10^{10} s^{-1} for $\omega = 15$ and 6.2×10^9 s^{-1} for $\omega = 1$. Although the decreases in the RMs from the bulk were similarly observed, it appears that the k_{rec} values in the *water-in-oil* RMs decrease with the decreasing micelle size, opposite to the previous reports with picosecond fluorescence measurements ($8.3 \times 10^8 \rightarrow 2.6 \times 10^9$ s^{-1} with $\omega = 20 \rightarrow 3$).[7] Fayer and co-workers attributed the increase of k_{rec} in the small micelles to the more significant probability of recombination between the detached proton and HPTS anion due to the limited space inside the RMs.[7] However, we speculate that the $k_{rec} = 8.3 \times 10^8$ s^{-1} reported for a large ($\omega = 20$) RMs can be inaccurate due to the relatively faster ESPT dynamics of HPTS compared to the time resolution of picosecond fluorescence measurements. Notably, our results of $k_{rec} = 6.2 \times 10^9$ s^{-1} for a small ($\omega = 1$) RMs are compatible with the value of 2.6×10^9 s^{-1} (for $\omega = 3$ RMs) reported by fluorescence measurements since the ESPT dynamics in the small RMs become largely slower than those in the large RMs and bulk. We consider the increases in the ratio of k_{rec} *vs.* k_{PT} from 1.6 to 2.1 with the micelle size decrease ($\omega = 15 \rightarrow 1$; 1.9 in bulk water) as the increased recombination probability in the small micelles. The reduction of the deprotonation dynamics of HPTS has also been observed in various confined environments, including cyclodextrin cavity, noisome, and lysosome of live cells.[52–55]

The deprotonation dynamics of HPTS in the *methanol-in-oil* RMs were similarly analyzed based on the time-resolved fluorescence measurements. The deprotonation of HPTS appears to occur in the *methanol-in-oil* RMs (especially in the small RMs), although the deprotonation was not observed in bulk methanol solution. We observed the deprotonation dynamics of HPTS becomes faster in both time constants (τ_1 and τ_2). The proton transfer rate constants (k_{PT}) of HPTS determined from the solution of eqn (1) are in the $5.8–9.1 \times 10^8$ s^{-1} range, which increases only with the small ($\omega = 1$) RMs. The recombination rate constants (k_{rec}) of HPTS in the *methanol-in-oil* RMs were determined as $2.7–9.6 \times 10^8$ s^{-1}, which also increases with the small ($\omega = 1–3$) RMs. HPTS in the *methanol-in-oil* RMs also showed increased recombination in the small RMs; the ratios of k_{rec} *vs.* k_{PT} increased $0.44 \rightarrow 1.1$ with the micelle size decrease ($\omega = 8 \rightarrow 1$). It is noted that the increased recombination rates of the contact ion pair in the small RMs due to the confinement are commonly observed with the water and methanol cores.

The dissociation rates (k_{diss}) of HPTS show apparent differences between the *water-in-oil* and *methanol-in-oil* RMs. The k_{diss} of HPTS in *water-in-oil* RMs is largely decreased from the bulk values with the minimum value of 1.3×10^9 s^{-1} for $\omega = 1$ RMs. On the other hand, the k_{diss} of HPTS in *methanol-in-oil* RMs appears to increase with the decrease of micelle size; the maximum value of 1.0×10^9 s^{-1} was obtained with the small ($\omega = 1$) RMs. The increased k_{diss} values of HPTS in the small *methanol-in-oil* RMs (comparable to the values in the *water-in-oil* RMs), in addition to a slight increase of k_{PT} compared to bulk ($6.6 \times 10^8 \rightarrow 9.1 \times 10^8$ s^{-1}), are considered strongly related to the appearance of anomalous deprotonation of HPTS in the small *methanol-in-oil* RMs.

Huppert and co-workers compared the k_{PT} values of photoacids in a wide acidity range in aqueous and alcoholic solutions.[44,57,78,90] Weak photoacids (p$K_a^* > 0$) show no deprotonation in protic solvents such as methanol and ethanol, while strong photoacids (p$K_a^* < 0$) deprotonate in the excited states. Interestingly, the k_{PT} values of a super-photoacid quinone cyanine 9 (p$K_a^* \sim -8.5$) were determined as 10^{13} s^{-1} with no difference between water, methanol, or ethanol. The solvent-independent ESPT dynamics of super-photoacids are considered

to be controlled by the solvation dynamics, where the activation barrier for the proton transfer is no longer relevant.[78,90,91] We report anomalous ESPT dynamics of a weak photoacid HPTS in small *methanol-in-oil* RMs. Similar k_{PT} values of 2.9×10^9 (for $\omega = 1$ *water-in-oil* RMs) and $9.1 \times 10^8 \text{ s}^{-1}$ (for $\omega = 1$ *methanol-in-oil* RMs) were observed from time-resolved fluorescence and transient absorption measurements. The k_{PT} values of HPTS in the order of 10^9 s^{-1} are strongly decreased from the value of $1.3 \times 10^{11} \text{ s}^{-1}$ in bulk aqueous solution, which represents that the ESPT of HPTS may be limited by the solvation dynamics of water in the nanopools of nonionic Igepal RMs. The solvation dynamics of confined water and methanol were determined as 3.7 and 2.6 ps for the small ($\omega = 1$) RMs from transient absorption measurements, which is compatible with previously reported values and largely increased from the bulk values (0.44 and 0.49 ps, respectively).[25,92] However, assigning the fastest kinetic components of transient absorption results as the solvation dynamics requires further consideration, as the proton transfer dynamics of photoacids in the RMs can be strongly perturbed by the limited solvation in the confined media inside the micelles. Experimental results of weaker and stronger photoacids would validate our interpretation regarding the anomalous solvent-independent proton transfer dynamics in the confined media of RMs.

The difference in the acidity (or basicity) of a chemical species between two solvents (or bulk and confined solvents in the RMs) by denoting the solvation energy changes (or free energy of transfer, ΔG_{tr}) of all the chemical species involved (HA, H$^+$, and A$^-$).[93] Cations and anions would show larger solvation energy transfer than neutral (protonated) species. Thus, the acidity of photo-excited HPTS in bulk methanol and *methanol-in-oil* RMs is strongly dependent on the solvation energy changes of the proton and deprotonated species of HPTS. Since the solvation dynamics (3.7 and 2.6 ps, respectively) and the proton transfer rate constant of HPTS ($k_{PT} \sim 10^9 \text{ s}^{-1}$) in the $\omega = 1$ RMs with the water and methanol core appear similar to each other, the solvation energy transfer in the RMs, $\Delta G_{tr,RM}$ of the proton and deprotonated species of HPTS may decrease from the bulk methanol solution ($\Delta G_{tr} = 10.4 \text{ kJ mol}^{-1}$ for H$^+$).[93] Thus, the acidity of photo-excited HPTS in the small RMs (either with water and methanol core) seems to decrease from the bulk aqueous solution or increased from the bulk methanol solution. Further experimental investigations on the acidity/basicity of confined methanol molecules in the RMs are needed to support our experimental results on the deprotonation of HPTS in small *methanol-in-oil* RMs and solvent-independent but micelle size-dependent deprotonation dynamics of (photo)acids.

In this work, we showed that the ESPT dynamics of a photoacid HPTS strongly depend on the heterogeneous environments of the nonionic RMs with water and methanol cores. In bulk solution, the deprotonation and intermolecular proton transfer of photoacids strongly depend on the acidity or basicity of solvents. However, the confined environments of the RMs with abnormally diminished solvent dynamics would make the ESPT dynamics of a weak photoacid HPTS almost insensitive to the acidity or basicity of solvents. Nonetheless, further experimental evidence with more or less strong photoacids is required to confirm that the ESPT in the polar cores of the nonionic RMs is mainly controlled by abnormally slower solvation dynamics in confined environments.

Conclusions

The proton transfer dynamics of a photoacid HPTS in the nonionic Igepal RMs with water and methanol cores have been extensively studied by steady-state and time-resolved electronic spectroscopy. Interestingly, the proton transfer of HPTS in the RMs shows opposite changes from the bulk, depending on the hydrophilic solvents in the core of the micelles. The deprotonation of HPTS strongly observed in the bulk aqueous solution becomes limited in the *water-in-oil* RMs with the micelle size decrease. However, the deprotonation of HPTS is observed in the small *methanol-in-oil* RMs, which does not occur in the bulk methanol solution. From the kinetic analysis of time-resolved fluorescence and transient absorption measurements, the proton transfer rate constants of HPTS in the *methanol-in-oil* RMs show anomalous increases with the micelle size decrease. In the small nonionic RMs, the proton transfer dynamics of HPTS become almost indistinguishable between the hydrophilic core of water and methanol. The abnormally slower solvation dynamics inside the nanoscopic pools of the RMs are considered to mainly control the ESPT dynamics of a weak photoacid HPTS, which appear insensitive to the acidity or basicity of core solvents. Nonionic RMs can be widely applicable for understanding the photodynamic properties of chromophores and biochemical reactions in biological environments, where the physical dimensions of the hydrophobic cavities or the electrostatic interactions with the interface can be considered crucial for the proton transfer dynamics of photoacids.

Author contributions

Conceptualization: T. J. and Y. P.; investigation: T. J. and S. L.; formal analysis: T. J. and S. L.; writing – original draft preparation: T. J. and Y. P.; writing-review and editing: Y.P.; supervision: Y. P.; all authors have read and agreed to the published version of the manuscript.

Conflicts of interest

There are no conflicts to declare.

Acknowledgements

11292 | *Phys. Chem. Chem. Phys.*, 2024, **26**, 11283–11294

This journal is © the Owner Societies 2024

References

1 P. Luisi, M. Giomini, M. A. Pileni and B. Robinson, *Biochim. Biophys. Acta, Rev. Biomembr.*, 1988, **947**, 209–246.

2 M. Pileni, *J. Phys. Chem.*, 1993, **97**, 6961–6973.

3 N. E. Levinger, *Science*, 2002, **298**, 1722–1723.

4 M. D. Fayer and N. E. Levinger, *Annu. Rev. Anal. Chem.*, 2010, **3**, 89–107.

5 N. E. Levinger and L. A. Swafford, *Annu. Rev. Phys. Chem.*, 2009, **60**, 385–406.

6 J. C. Deàk, Y. Pang, T. D. Sechler, Z. Wang and D. D. Dlott, *Science*, 2004, **306**, 473–476.

7 C. Lawler and M. D. Fayer, *J. Phys. Chem. B*, 2015, **119**, 6024–6034.

8 T. Jang, G. Lee, S. Lee, J. Lee and Y. Pang, *J. Mol. Liq.*, 2019, **279**, 503–509.

9 G. Lee, T. Jang, S. Lee, H. Oh, H. Lee and Y. Pang, *J. Mol. Liq.*, 2020, **305**, 112873.

10 M. Sedgwick, R. L. Cole, C. D. Rithner, D. C. Crans and N. E. Levinger, *J. Am. Chem. Soc.*, 2012, **134**, 11904–11907.

11 M. Giustini, G. Palazzo, G. Colafemmina, M. Della Monica, M. Giomini and A. Ceglie, *J. Phys. Chem.*, 1996, **100**, 3190–3198.

12 D. M. Zhu, K. I. Feng and Z. A. Schelly, *J. Phys. Chem.*, 1992, **96**, 2382–2385.

13 S. Lipgens, D. Schübel, L. Schlicht, J. H. Spilgies, G. Ilgenfritz, J. Eastoe and R. K. Heenan, *Langmuir*, 1998, **14**, 1041–1049.

14 M. Vasilescu, A. Caragheorgheopol, M. Almgren, W. Brown, J. Alsins and R. Johannsson, *Langmuir*, 1995, **11**, 2893–2898.

15 E. Gaidamauskas, D. P. Cleaver, P. B. Chatterjee and D. C. Crans, *Langmuir*, 2010, **26**, 13153–13161.

16 N. Sarkar, K. Das, A. Datta, S. Das and K. Bhattacharyya, *J. Phys. Chem.*, 1996, **100**, 10523–10527.

17 J. Faeder and B. M. Ladanyi, *J. Phys. Chem. B*, 2001, **105**, 11148–11158.

18 J. Chowdhary and B. M. Ladanyi, *J. Phys. Chem. B*, 2009, **113**, 15029–15039.

19 I. V. Kopanichuk, A. A. Vanin, A. Ostras' and E. N. Brodskaya, *Colloid J.*, 2018, **80**, 266–271.

20 N. M. Correa, J. J. Silber, R. E. Riter and N. E. Levinger, *Chem. Rev.*, 2012, **112**, 4569–4602.

21 Z. Li and G. A. Voth, *Phys. Chem. Chem. Phys.*, 2020, **22**, 10753–10763.

22 A. D'Aprano, A. Lizzio, V. T. Liveri, F. Aliotta, C. Vasi and P. Migliardo, *J. Phys. Chem.*, 1988, **92**, 4436–4439.

23 R. Costard, N. E. Levinger, E. T. J. Nibbering and T. Elsaesser, *J. Phys. Chem. B*, 2012, **116**, 5752–5759.

24 P. Hazra, D. Chakrabarty and N. Sarkar, *Chem. Phys. Lett.*, 2003, **371**, 553–562.

25 E. E. Fenn, D. B. Wong, C. H. Giammanco and M. D. Fayer, *J. Phys. Chem. B*, 2011, **115**, 11658–11670.

26 D. M. Vriezema, M. Comellas Aragonès, J. A. A. W. Elemans, J. J. L. M. Cornelissen, A. E. Rowan and R. J. M. Nolte, *Chem. Rev.*, 2005, **105**, 1445–1490.

27 J. Eastoe, M. J. Hollamby and L. Hudson, *Adv. Colloid Interface Sci.*, 2006, **128–130**, 5–15.

28 B. S. Marques, N. V. Nucci, I. Dodevski, K. W. C. Wang, E. A. Athanasoula, C. Jorge and A. J. Wand, *J. Phys. Chem. B*, 2014, **118**, 2020–2031.

29 R. W. Peterson, K. Anbalagan, C. Tommos and A. J. Wand, *J. Am. Chem. Soc.*, 2004, **126**, 9498–9499.

30 A. S. Narang, D. Delmarre and D. Gao, *Int. J. Pharm.*, 2007, **345**, 9–25.

31 H.-W. Nho, J.-H. Park, A. Adhikari and O.-H. Kwon, *J. Mol. Liq.*, 2021, **326**, 115270.

32 D. C. Crans and N. E. Levinger, *Acc. Chem. Res.*, 2012, **45**, 1637–1645.

33 O. A. El Seoud, A. M. Chinelatto and M. R. Shimizu, *J. Colloid Interface Sci.*, 1982, **88**, 420–427.

34 M. Hasegawa, *Langmuir*, 2001, **17**, 1426–1431.

35 M. da Graça Miguel, H. D. Burrows, M. A. Escaroupa Pereira and A. P. Varela, *Colloids Surf., A*, 2001, **176**, 85–99.

36 N. A. Vodolazkaya, N. O. McHedlov-Petrossyan, N. V. Salamanova, Y. N. Surov and A. O. Doroshenko, *J. Mol. Liq.*, 2010, **157**, 105–112.

37 B. Baruah, J. M. Roden, M. Sedgwick, N. M. Correa, D. C. Crans and N. E. Levinger, *J. Am. Chem. Soc.*, 2006, **128**, 12758–12765.

38 M. A. Sedgwick, D. C. Crans and N. E. Levinger, *Langmuir*, 2009, **25**, 5496–5503.

39 O. F. Mohammed, D. Pines, J. Dreyer, E. Pines and E. T. J. Nibbering, *Science*, 2005, **310**, 83–86.

40 D. B. Spry, A. Goun and M. D. Fayer, *J. Phys. Chem. A*, 2007, **111**, 230–237.

41 C. Spies, S. Shomer, B. Finkler, D. Pines, E. Pines, G. Jung and D. Huppert, *Phys. Chem. Chem. Phys.*, 2014, **16**, 9104–9114.

42 T. Kumpulainen, B. Lang, A. Rosspeintner and E. Vauthey, *Chem. Rev.*, 2017, **117**, 10826–10939.

43 L. M. Tolbert and K. M. Solntsev, *Acc. Chem. Res.*, 2002, **35**, 19–27.

44 N. Agmon, D. Huppert, A. Masad and E. Pines, *J. Phys. Chem.*, 1991, **95**, 10407–10413.

45 K. J. Tielrooij, M. J. Cox and H. J. Bakker, *ChemPhysChem*, 2009, **10**, 245–251.

46 A. Phukon and K. Sahu, *Chem. Commun.*, 2015, **51**, 14103–14106.

47 A. Phukon, N. Barman and K. Sahu, *Langmuir*, 2015, **31**, 12587–12596.

48 R. Nandi and N. Amdursky, *Acc. Chem. Res.*, 2022, **55**, 2728–2739.

49 O. F. Mohammed, J. Dreyer, B.-Z. Magnes, E. Pines and E. T. J. Nibbering, *ChemPhysChem*, 2005, **6**, 625–636.

50 T. H. Tran-Thi, T. Gustavsson, C. Prayer, S. Pommeret and J. T. Hynes, *Chem. Phys. Lett.*, 2000, **329**, 421–430.

51 W. Heo, N. Uddin, J. W. Park, Y. M. Rhee, C. H. Choi and T. Joo, *Phys. Chem. Chem. Phys.*, 2017, **19**, 18243–18251.

52 S. S. Mojumdar, R. Chowdhury, A. K. Mandal and K. Bhattacharyya, *J. Chem. Phys.*, 2013, **138**, 215102.

53 S. K. Mondal, K. Sahu, P. Sen, D. Roy, S. Ghosh and K. Bhattacharyya, *Chem. Phys. Lett.*, 2005, **412**, 228–234.

54 T. Mondal, S. Ghosh, A. K. Das, A. K. Mandal and K. Bhattacharyya, *J. Phys. Chem. B*, 2012, **116**, 8105–8112.

This journal is © the Owner Societies 2024

Phys. Chem. Chem. Phys., 2024, **26**, 11283–11294 | 11293

55 R. Chowdhury, A. Saha, A. K. Mandal, B. Jana, S. Ghosh and K. Bhattacharyya, *J. Phys. Chem. B*, 2015, **119**, 2149–2156.

56 J. E. Thomaz, A. R. Walker, S. J. Van Wyck, J. Meisner, T. J. Martinez and M. D. Fayer, *J. Phys. Chem. B*, 2020, **124**, 7897–7908.

57 I. Carmeli, D. Huppert, L. M. Tolbert and J. E. Haubrich, *Chem. Phys. Lett.*, 1996, **260**, 109–114.

58 Y. M. Lee, S.-Y. Park, H. Kim, T. G. Kim and O.-H. Kwon, *Methods Appl. Fluoresc.*, 2016, **4**, 024004.

59 A. Brenlla, M. Veiga Gutiérrez, M. C. Ríos Rodríguez, F. Rodríguez-Prieto, M. Mosquera and J. L. Pérez Lustres, *J. Phys. Chem. Lett.*, 2014, **5**, 989–994.

60 P. Verma, A. Rosspeintner, B. Dereka, E. Vauthey and T. Kumpulainen, *Chem. Sci.*, 2020, **11**, 7963–7971.

61 R. E. Riter, J. R. Kimmel, E. P. Undiks and N. E. Levinger, *J. Phys. Chem. B*, 1997, **101**, 8292–8297.

62 C. G. Elles and N. E. Levinger, *Chem. Phys. Lett.*, 2000, **317**, 624–630.

63 P. Setua, D. Seth and N. Sarkar, *Phys. Chem. Chem. Phys.*, 2009, **11**, 8913–8922.

64 A. Shabbir, T. Jang, G. Lee and Y. Pang, *J. Mol. Liq.*, 2022, **346**, 118313.

65 P. Hazra, D. Chakrabarty and N. Sarkar, *Chem. Phys. Lett.*, 2002, **358**, 523–530.

66 P. Hazra and N. Sarkar, *Phys. Chem. Chem. Phys.*, 2002, **4**, 1040–1045.

67 A. A. Awasthi and P. K. Singh, *ChemPhysChem*, 2018, **19**, 198–207.

68 N. Sülzner and C. Hättig, *J. Phys. Chem. A*, 2022, **126**, 5911–5923.

69 S. K. K. Kumar, A. Tamimi and M. D. Fayer, *J. Am. Chem. Soc.*, 2013, **135**, 5118–5126.

70 D. Lee, J. Lee, J. Song, M. Jen and Y. Pang, *Phys. Chem. Chem. Phys.*, 2019, **21**, 11599–11607.

71 G. R. Fleming, J. M. Morris and G. W. Robinson, *Chem. Phys.*, 1976, **17**, 91–100.

72 J. Lee, J. Song, D. Lee and Y. Pang, *Sci. Rep.*, 2019, **9**, 3551.

73 J. J. Snellenburg, S. P. Laptenok, R. Seger, K. M. Mullen and I. H. M. Stokkun, *J. Stat. Softw.*, 2012, **49**, 1–22.

74 M. J. Politi, O. Brandt and J. H. Fendler, *J. Phys. Chem.*, 1985, **89**, 2345–2354.

75 S. Singh, S. Koley, K. Mishra and S. Ghosh, *J. Phys. Chem. C*, 2018, **122**, 732–740.

76 E. Pines and D. Huppert, *J. Chem. Phys.*, 1986, **84**, 3576–3577.

77 F. Rived, M. Rosés and E. Bosch, *Anal. Chim. Acta*, 1998, **374**, 309–324.

78 R. Simkovitch, S. Shomer, R. Gepshtein and D. Huppert, *J. Phys. Chem. B*, 2015, **119**, 2253–2262.

79 G. Fonrodona, C. Ràfols, E. Bosch and M. Rosés, *Anal. Chim. Acta*, 1996, **335**, 291–302.

80 N. Nandi and K. Sahu, *J. Photochem. Photobiol., A*, 2019, **374**, 138–144.

81 D. B. Spry, A. Goun, K. Glusac, D. E. Moilanen and M. D. Fayer, *J. Am. Chem. Soc.*, 2007, **129**, 8122–8130.

82 T. Mondal, A. K. Das, D. K. Sasmal and K. Bhattacharyya, *J. Phys. Chem. B*, 2010, **114**, 13136–13142.

83 Y. Wang, W. Liu, L. Tang, B. Oscar, F. Han and C. Fang, *J. Phys. Chem. A*, 2013, **117**, 6024–6042.

84 R. Simkovitch, G. G. Rozenman and D. Huppert, *J. Photochem. Photobiol., A*, 2017, **344**, 15–27.

85 G. M. Sando, K. Dahl and J. C. Owrutsky, *J. Phys. Chem. A*, 2004, **108**, 11209–11217.

86 D. Pant and N. E. Levinger, *Langmuir*, 2000, **16**, 10123–10130.

87 P. Leiderman, L. Genosar and D. Huppert, *J. Phys. Chem. A*, 2005, **109**, 5965–5977.

88 L. Giestas, C. Yihwa, J. C. Lima, C. Vautier-Giongo, A. Lopes, A. L. Maçanita and F. H. Quina, *J. Phys. Chem. A*, 2003, **107**, 3263–3269.

89 S. Senapati and A. Chandra, *J. Phys. Chem. B*, 2001, **105**, 5106–5109.

90 R. Simkovitch, S. Shomer, R. Gepshtein, M. E. Roth, D. Shabat and D. Huppert, *J. Photochem. Photobiol., A*, 2014, **277**, 90–101.

91 J. Pérez-Lustres, F. Rodriguez-Prieto, M. Mosquera, T. Senyushkina, N. Ernsting and S. Kovalenko, *J. Am. Chem. Soc.*, 2007, **129**, 5408–5418.

92 D. E. Moilanen, N. E. Levinger, D. B. Spry and M. D. Fayer, *J. Am. Chem. Soc.*, 2007, **129**, 14311–14318.

93 B. G. Cox, *Acids and Bases: Solvent Effects on Acid–Base Strength*, Oxford University Press, 2013.

11294 | *Phys. Chem. Chem. Phys.*, 2024, **26**, 11283–11294

This journal is © the Owner Societies 2024